

# Insights into the Water Transport Mechanism in Polymeric Membranes from Neutron Scattering<sup>†</sup>

Edwin P. Chan,<sup>\*,‡</sup> Bradley R. Frieberg,<sup>‡</sup> Kanae Ito,<sup>‡</sup> Jacob Tarver,<sup>¶,§</sup> Madhusudan Tyagi,<sup>¶,||</sup> Wenxu Zhang,<sup>⊥</sup> E. Bryan Coughlin,<sup>#</sup> Christopher M. Stafford,<sup>‡</sup> Abhishek Roy,<sup>@</sup> Steve Rosenberg,<sup>@</sup> and Christopher L. Soles<sup>\*,‡</sup>

<sup>‡</sup>*Materials Science and Engineering Division, National Institute of Standards and Technology, Gaithersburg, MD 20899*

<sup>¶</sup>*NIST Center for Neutron Research, National Institute of Standards and Technology, Gaithersburg, MD 20899*

<sup>§</sup>*Department of Materials Science and Engineering, University of Maryland, College Park, MD 20742*

<sup>||</sup>*National Renewable Energy Laboratory, Golden, CO 80401*

<sup>⊥</sup>*Department of Chemistry, Massachusetts Institute of Technology, Cambridge, MA 02139*

<sup>#</sup>*Polymer Science and Engineering Department, University of Massachusetts, Amherst, MA 01003*

<sup>@</sup>*Energy and Water Solutions, Dow Chemical Company, Edina, MN 55439*

E-mail: edwin.chan@nist.gov; christopher.soles@nist.gov

Phone: 301-975-5228; 301-975-8087. Fax: 301-975-4942

---

<sup>†</sup>Edwin P. Chan and Bradley R. Frieberg contributed equally to this work

## Abstract

Polymeric membranes are ubiquitous in transport applications including gas separation, water desalination, solid state batteries and fuel cells. The transport mechanism in certain classes of membranes is well understood. It is generally believed that polymeric membranes used in gas separation follow the solution-diffusion model.<sup>1</sup> However, the transport mechanism in other membranes such as ones used in water desalination is less clear as both the solution-diffusion<sup>2,3</sup> and the hydrodynamic<sup>4,5</sup> model have been proposed. In this contribution, we study the structure as well as the water and polymer dynamics of several polymeric membranes using small-angle and quasi-elastic neutron scattering. We demonstrate that on the scale of a few nanometers, water appears to diffuse through a water desalination membrane at a rate comparable to bulk water, while water diffuses at a rate that is a factor of two slower in an anion exchange membrane. These results illustrate the importance of studying both the structure and dynamics of membrane materials but also have important implications in understanding the underlying transport mechanisms that differentiate different types of polymeric membranes.

## Introduction

Transport in polymeric membrane materials is generally described by two primary models with distinct relationships with the polymer structure.<sup>6,7</sup> The first describes transport in polymers as a solution-diffusion process where the permeant first solubilizes into the membrane and then diffuses across it due to a concentration gradient. The second is the hydrodynamic model, which describes the transport of a permeant as a pressure-driven process through physical pores with a characteristic pore size,  $\xi$ . Since this model follows a convective mechanism, the number density, dimensionality and connectivity of the pores determine the rate of transport.

Previous studies on water desalination membranes have proposed both the solution-diffusion<sup>2,3</sup> and the hydrodynamic<sup>4,5</sup> model to describe water transport in these materials.

Much of this debate is attributed to the challenges associated with measuring the transport properties of these materials at the nanoscale. It is very difficult to directly measure their intrinsic transport properties as they are engineered to be as thin as possible, thus the mechanism of transport for most membranes are inferred based on extrinsic permeation measurements.<sup>8</sup>

One particular measurement platform that can measure the transport dynamics at such small length- and time-scales is quasi-elastic neutron scattering, a technique that measures the scattering intensity of dynamic processes as a function of both scattering vector ( $Q$ ) and energy transfer ( $E$ ). The technique is ideally suited for studying water and polymer chain dynamics related to the functional layer of the membrane because it can resolve motions of hydrogenous species on length-scales of several nanometers and time-scales on the order of nano- to picosecond; these are the appropriate length and time-scales for discerning the different molecular transport models relevant to membrane materials.

In this study, we apply small-angle neutron scattering (SANS) and quasi-elastic neutron scattering (QENS) to investigate two representative polymeric membranes. The first is a triblock copolymer-based anion exchange membrane of poly(vinylbenzyltrimethylammonium chloride-*b*-cyclooctene-*b*-vinylbenzyltrimethylammonium chloride) (P(VBTMA-*b*-COE-*b*-VBTMA)) that is typically used in alkaline fuel cells, which we will simply refer to as an anion exchange membrane (AEM) (Fig. 1a). The second material is a crosslinked aromatic polyamide of poly(*m*-phenylenediamine trisamide) (PMPDTA) that is traditionally used in water desalination applications, which we will refer to as a desalination membrane (DM) (Fig. 1b). We show that on the nanometer length-scale, water diffuses through the AEM at a rate that is a factor of two slower than bulk water. On the other hand, water diffuses through the DM at a rate similar to bulk water. We reconcile these results in the context of the different dynamics related to water transport, as studied by QENS, of the two membrane materials.

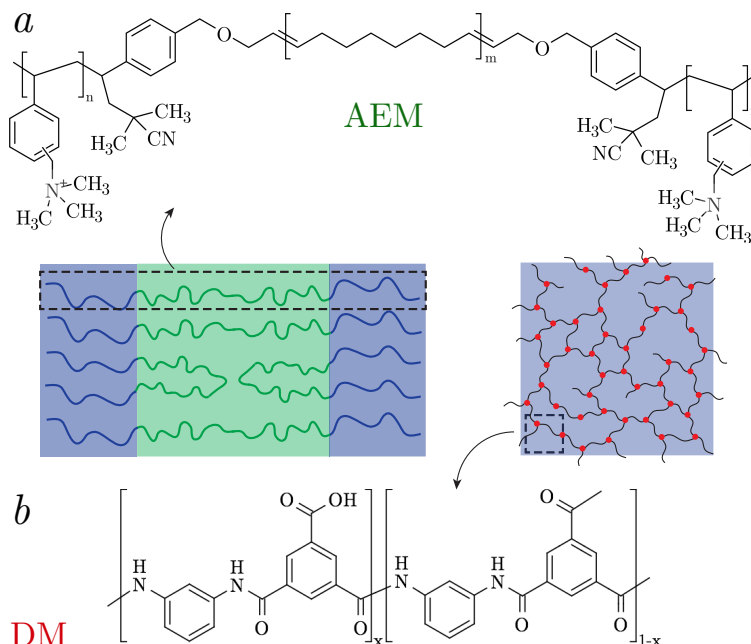


Figure 1: Chemical structures of the polymer membranes investigated in this work. a) The AEM is a triblock copolymer anion exchange membrane used in alkaline fuel cells. b) The DM is a crosslinked aromatic polyamide used in water desalination.

## Experimental

Certain instruments and materials are identified in this paper to adequately specify the experimental details. Such identification does not imply recommendation by the National Institute of Standards and Technology; nor does it imply that the materials are necessarily the best available for the purpose.

## Materials

The DM was provided by Dow FilmTec. The DM functional layer was removed from the mechanical support layers via a process previously described.<sup>9</sup> Hundreds of selective layers were recovered and stacked in an aluminum foil pouch to obtain a total sample mass of  $\approx 100$  mg. The AEM used in this study was prepared by the following procedure. First, poly(chloromethylstyrene-*b*-cyclooctene-*b*-chloromethylstyrene) was synthesized by sequential Chain-Transfer Ring-Opening Metathesis Polymerization and Reversible Addition-

Fragmentation Chain Transfer Radical Polymerization.<sup>10</sup> Then the copolymer was cast from chloroform solution (10% by mass) onto a Teflon sheet and dried slowly at room temperature. The film was peeled off and dipped in a trimethylamine solution (50% by mass in H<sub>2</sub>O), before being annealed in pure water at 353 K for two days. The AEM films (100  $\mu$ m thick) were cast from solution and then transferred to aluminum foil. The AEM used in this study is a lamellar forming block copolymer with a hydrophobic cyclooctene block and a hydrophilic styrene-TMA block. When hydrated, the water molecules will preferentially segregate in the ionic domains to generate unique conduction channels.

Both sample sets were first dried under vacuum overnight to remove excess water. The samples were annealed at 393 K for two hours to fully remove any excess water. The samples were then hydrated for two hours at room temperature in a Nitrogen filled environment with a saturated salt solution to maintain the desired humidity: Magnesium chloride  $\approx$  30% RH, potassium chloride  $\approx$  80% RH, and water  $\approx$  100% RH. The approximate mass uptake of water was monitored by measuring the hydrated mass relative to the dry sample mass. The H<sub>2</sub>O hydrated samples were then loaded in air with a reservoir of same saturated salt solution loaded at the bottom of the sample can. The reservoir was maintained so that it was not in contact with the sample and was out of the direct neutron beam. The D<sub>2</sub>O hydrated samples were loaded while in a nitrogen filled glove box, also with a saturated salt solution at the bottom of the sample can. The samples were then equilibrated for 6 hours prior to measurement.

## Neutron Scattering Measurements

Neutron scattering experiments were conducted at the NIST Center for Neutron Research (NCNR). The structure of the membranes was probed using small angle neutron scattering (SANS) on the 10 m SANS beamline operated by Neutrons for Soft Matter (nSOFT). The SANS spectra were generated using three instrument configurations by controlling the sample

detector distance (SSD) and neutron wavelength ( $\lambda$ ), which are 1. SDD=1.2 m,  $\lambda = 5$  Å, 2. SDD=5.2 m  $\lambda = 5$  Å, and SDD=5.2 m,  $\lambda = 10$  Å. The samples were measured within the aluminum sample holders used for the quasi-elastic neutron scattering (QENS) measurements. The signal was corrected for detector sensitivity, background counts and scattering from the aluminum can. The intensity was scaled using the empty beam flux. The SANS data was reduced using Igor Macros provided by NCNR.<sup>11</sup> The SANS data was then analyzed using SasView.

We used QENS, a form of inelastic scattering, to probe the water and polymer membrane dynamics. QENS measurements were made on multiple spectrometers to span orders of magnitude in time scales from tens of picoseconds to nanoseconds. The QENS spectra was collected at several different temperatures, at and above room temperature, that are relevant to the operation conditions of the respective membranes. The polymer membrane dynamics were probed using the high flux backscatter spectrometer (HFBS) with an energy resolution of 1  $\mu\text{eV}$  and an energy window of  $\pm 15$   $\mu\text{eV}$ . The faster water dynamics were probed using the disk chopper time-of-flight spectrometer (DCS) with an incident neutron wavelength ( $\lambda$ ) of 9 Å, which yields an energy resolution of 22  $\mu\text{eV}$  and the energy window was limited to  $\pm 0.5$   $\text{meV}$ . The instrument resolution on both spectrometers was measured using a vanadium standard. The data reduction and analysis was performed using the DAVE software package.<sup>12</sup>

## Results and discussion

Prior studies on the macroscopic water uptake of these membrane materials reveal very distinct swelling behavior. The water uptake for a hydrated AEM is  $\approx (10 - 20)\%$  by mass with the swelling behavior suggested to proceed via volumetric expansion of the PVBTMA block;<sup>10</sup> water does not solubilize in the hydrophobic PCOE block. The maximum water uptake for DM is  $< 5\%$  by mass at maximum water vapor activity ( $\approx 96\%$  RH),<sup>13,14</sup> which

is lower than the maximum swelling of the AEM. Compared with conventional glassy polymers with minimal swelling ( $< 1\%$ ), the AEM swells significantly whereas the DM swells moderately. Since the network structure of these DM materials is fairly rigid with significant amount of network heterogeneities consisting of unreacted functional groups,<sup>15</sup> it has been suggested that they swell primarily via topological rearrangement related to these cross-linking heterogeneities.<sup>13,14</sup> In the fully crosslinked regions, the swelling is minimal and is comparable with that of a polymer glass. On the other hand, there is significant expansion near the less crosslinked parts of the material upon exposure to water.

SANS studies of these materials in dry and D<sub>2</sub>O hydrated conditions, which significantly enhances the neutron scattering contrast between the polymer and water, confirm their unique swelling mechanism. The scattering intensity ( $I(Q)$ ) vs. scattering vector ( $Q$ ) curves for the AEM are shown in Fig. 2. We fit all of the SANS curves with the following model<sup>16</sup> consisting of correlation lengths  $\xi_1$  and  $\xi_2$ ,

$$I(Q) = \frac{A}{Q^p} + \frac{C}{1 + (Q\xi_1)^{l_1}} + \frac{D}{1 + (Q\xi_2)^{l_2}} + B. \tag{1}$$

where  $p$  is the Porod exponent,  $l_1$  and  $l_2$  are the Lorentz exponents. **Eq. 1 was used to describe the SANS results in order to identify the unique length-scales present in these swollen polymer films. Similar forms of Eq. 1 have been used by others to describe the SANS results for polymer gels with spatial heterogeneities.**<sup>17-19</sup> Detailed fits to extrapolate the correlation lengths for both AEM and DM are shown in the Supporting Information section. The values for the fitting coefficients are summarized in Table 1.

Table 1: Extrapolated parameters for fits to the SANS measurements for AEM and DM.

	$p$	$l_1$	$l_2$	$\xi_1$ (Å)	$\xi_2$ (Å)
AEM dry	$2.36 \pm 0.18$	$3.44 \pm 1.33$	$3.78 \pm 2.38$	$57.1 \pm 3.4$	$25.7 \pm 0.2$
AEM D <sub>2</sub> O hyd.	$4.02 \pm 0.29$	$4.22 \pm 0.13$	$3.75 \pm 0.11$	$63.8 \pm 0.6$	$28.0 \pm 2.8$
DM dry	$3.66 \pm 0.05$	$4.20 \pm 0.01$	$4.19 \pm 0.03$	$87.5 \pm 0.4$	$26.0 \pm 0.9$
DM D <sub>2</sub> O hyd.	$3.69 \pm 0.02$	$4.18 \pm 0.01$	$3.93 \pm 0.01$	$89.6 \pm 1.1$	$26.8 \pm 0.1$

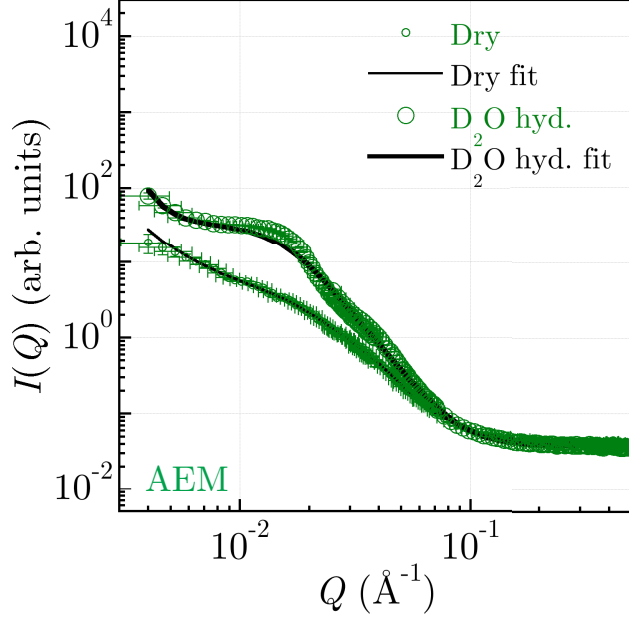


Figure 2: SANS results, along with fits, of the dry and D<sub>2</sub>O hydrated AEM.

The SANS results for AEM indicate the presence of two correlation lengths ( $\xi_1=57.1 \text{ \AA}$ ,  $\xi_2=25.7 \text{ \AA}$ ) in the dry state.  $\xi_1$  is consistent with the block copolymer microdomain spacing<sup>10</sup> and we attribute  $\xi_2$  to be associated with the higher order scattering of the primary peak. Upon swelling with D<sub>2</sub>O, this correlation length increases to  $\xi_1=63.8 \text{ \AA}$ , which is approximately a 10% increase, which translates to  $\approx 23\%$  water content within the ionic PVBTMA microdomain at maximum swelling. Additionally, the increase in scattering intensity of both the primary and secondary peak is consistent with an enhancement in the scattering contrast of the swollen block copolymer.

The SANS results for DM were also adequately fit with the two correlation length ( $\xi_1=87.5 \text{ \AA}$ ,  $\xi_2=26.0 \text{ \AA}$ ) model in the dry state. Interestingly, these correlation lengths only increase slightly upon swelling with D<sub>2</sub>O. Assuming that  $\xi_1$  and  $\xi_2$  are related to the length-scales of the network heterogeneities within the DM, it would suggest these nanoscale heterogeneities in the dry state do not change significantly, with  $\approx 2 \%$  increase, in size with hydration.

SANS supports the notion of selective hydration and swelling of one of the domains in the AEM whereas the swelling of the DM appears to be more uniform; a new length scale in

the structure does not appear upon hydration. Therefore, the SANS results reveal a static picture of the structure of these materials but does not enable us to elucidate the specific transport mechanism. To study the transport dynamics, we measure these materials using QENS at several temperatures at and above room temperature. QENS is an incoherent scattering technique that is ideally suited for studying water and polymer dynamics since the measured signal is dominated by the inelastic scattering of the hydrogen atoms as the incoherent neutron scattering cross section of hydrogen is at least 40 times larger than deuterium, oxygen, nitrogen and carbon. Two spectrometers were used to probe the polymer and water dynamics for this study. The slow dynamics were probed using the high flux backscatter spectrometer (HFBS) with an energy resolution of  $1 \mu\text{eV}$  and an energy window of  $\pm 15 \mu\text{eV}$ .<sup>20</sup> The faster water dynamics were probed using the disk chopper time-of-flight spectrometer (DCS) with an energy resolution of  $22 \mu\text{eV}$  and the energy window was limited to  $\pm 0.5 \text{ meV}$ .<sup>21</sup>

Fig. 3 shows the dynamic structure factor ( $S(Q, \omega)$ ) vs.  $Q$  curves for AEM from the HFBS and DCS spectrometers. We use the following equation to fit the curves,

$$S(Q, \omega) = I(Q) \left( xR(\omega) + x_1R(\omega) \otimes L_p(\omega) \right. \\ \left. + (1 - x - x_1)R(\omega) \otimes L_w(\omega) \right) + B, \quad (2)$$

Here,  $I(Q)$  is the scaled intensity at a given  $Q$ ,  $R(\omega)$  is the resolution function of the instrument,  $L_p(\omega)$  is the Lorentzian distribution associated with the polymer motions, and  $L_w(\omega)$  is the Lorentzian distribution associated with the water motions and  $B$  is a flat background. The value  $x$  corresponds to the elastic incoherent structure factor ( $EISF$ ) and  $x_1$  is the fraction of the dynamics corresponding to motions in the polymer. The motions of the polymer and water, both described as Lorentzian distributions, are convoluted with the instrumental resolution.

Since there are hydrogen atoms in the  $\text{H}_2\text{O}$  as well as along the polymer backbone, the motions from both of these moieties will be observed in a QENS spectra for a  $\text{H}_2\text{O}$  hydrated

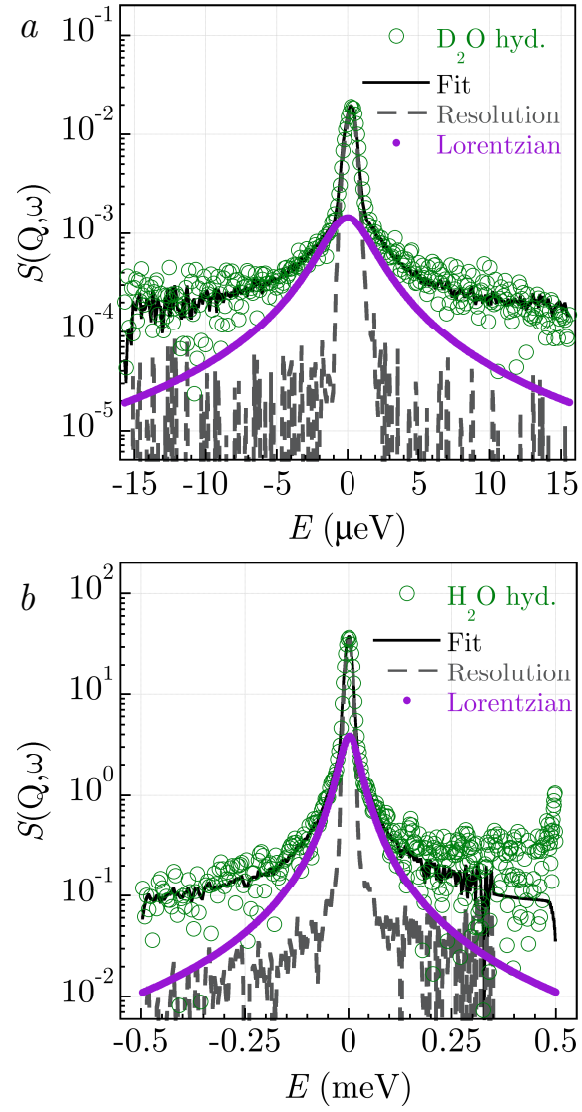


Figure 3: Dynamic structure factor ( $S(Q, w)$ ), along with fits, of the hydrated AEM from QENS at  $Q = 1 \text{ \AA}^{-1}$ . a)  $S(Q, w)$  from HFBS for AEM that is hydrated with  $\text{D}_2\text{O}$ . b)  $S(Q, w)$  from DCS for AEM hydrated with  $\text{H}_2\text{O}$ .

sample. To deconvolute the hydrogen motions of the polymer backbone from that of the water molecules, we also conducted HFBS measurements of the same samples hydrated with D<sub>2</sub>O under identical conditions. The HFBS spectra for AEM hydrated with D<sub>2</sub>O at 80% RH shows a broad fast process and a slower narrow process associated with the energy resolution of the instrument (Fig. 3a). The motions are adequately described by a single Lorentzian associated with the dynamics of just the hydrated polymer, and Eq. 2 simplifies to,

$$S(Q, \omega) = I(Q) \left( xR(\omega) + (1 - x)R(\omega) \otimes L(\omega) \right) + B. \quad (3)$$

The slower motions associated with the polymer dynamics were determined by fitting the D<sub>2</sub>O hydrated sample to Eq. 3. From the fit in this sample we obtain  $L(\omega)$  and  $x$ , the Lorentzian describing polymer motions and fraction of immobile hydrogen atoms. It is assumed that the polymer dynamics will not be significantly influenced by switching from D<sub>2</sub>O to H<sub>2</sub>O. When fitting the H<sub>2</sub>O hydrated sample,  $L_p(Q)$  was held fixed at the values from the D<sub>2</sub>O sample,  $L(Q)$ . Therefore, the only free variables for this sample was  $L_w(\omega)$  and the relative fraction of immobile hydrogen atoms,  $x$ , and relative fraction of hydrogen atoms associated with polymer motions,  $x_1$ . The Lorentzian function associated with water dynamics,

$$L_w(\omega) = \frac{\Gamma_w(Q)}{\pi(\Gamma_w(Q)^2 + \omega^2)}, \quad (4)$$

can be described by the half width half maximum,  $\Gamma_w(Q)$ , centered around 0 energy transfer. Comparing the spectra for the H<sub>2</sub>O hydrated with the D<sub>2</sub>O hydrated AEM (see Supporting Information), it is evident that the broad fast process of the water motions is almost beyond the range of the HFBS spectrometer. Therefore, to fully understand the water diffusion process, similar experiments and fitting routines were also conducted using DCS to capture motions on a faster time-scale.

For DM, we didn't observe any appreciable motions associated with polymer or H<sub>2</sub>O

dynamics within the time-scale of the HFBS measurement and the spectra are included in the Supporting Information section. This observation indicates that the DM network structure is relatively static on the nanosecond time-scale of the HFBS measurement and supports the interpretation from the SANS results that the network structure does not change significantly even when saturated with water. It also suggests that water inside the DM is moving faster than the time-scale of the HFBS spectrometer.

Fig. 3b shows the DCS spectra for the H<sub>2</sub>O hydrated AEM membrane at  $Q = 1.0 \text{ \AA}^{-1}$  at room temperature. Within the energy window of  $\pm 0.5 \text{ meV}$ , we fit the data with a single Lorentzian distribution that is associated with the motions of the water molecules. Comparing the DCS spectra of the two membranes (see Supporting Information), the relative broadness of the Lorentzian distribution indicates that the water dynamics is significantly faster for DM compared to AEM.

We quantify the water dynamics within the membranes by characterizing the  $Q$  dependence of  $\Gamma_w$  as shown in Fig. 4. If the water molecules observe simple Fickian diffusion,  $\Gamma_w$  would scale linearly with  $Q^2$ , i.e.  $\Gamma_w \propto D_w Q^2$ , where  $D_w$  is the self-diffusion coefficient of water. This could be the case at low  $Q$  but  $\Gamma_w$  clearly turns over into a plateau at higher  $Q^2$  values. This high  $Q$  turnover is indicative of a jump diffusion process, where the water molecules are confined at short time- and length-scales but experience diffusive jumps at longer time- and length-scales.

We fit our materials using the Hall and Ross model that assumes the motions as unconstrained random jump diffusion processes with a Gaussian distribution of jump lengths.<sup>22</sup> This model predicts the quasi-elastic broadening as,

$$\Gamma(Q) = \frac{1}{\tau} \left( 1 - e^{-Q^2 \langle l^2 \rangle / 6} \right). \quad (5)$$

with a residence time between jumps of  $\tau$  and a mean squared jump length of  $\langle l^2 \rangle$ . At sufficiently large length-scales, this model predicts linear Fickian-like diffusion in the low  $Q$

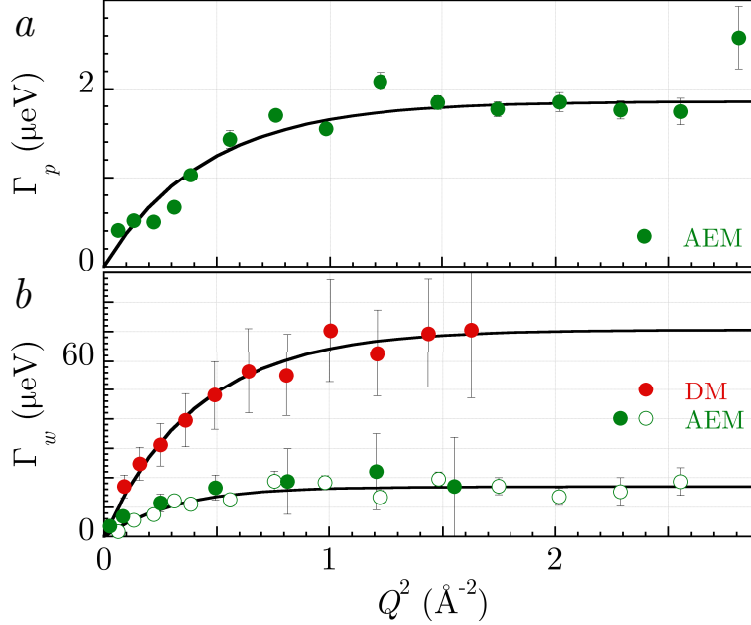


Figure 4: a)  $\Gamma_p(Q)$  for AEM hydrated with  $\text{H}_2\text{O}$ . b)  $\Gamma_w(Q)$  for DM and AEM hydrated with  $\text{H}_2\text{O}$ . Error bars represent one standard deviation.

regime, and asymptotes to  $2/\tau$  in the high  $Q$  regime. It is evident that Eq. 5 appropriately captures the data (Fig. 4). The fitting parameters (Table 2) indicate that  $\langle l^2 \rangle$  was independent of temperature ( $T$ ) within the temperature range investigated. The jump length for DM was found to be  $\langle l \rangle \approx 3 \text{ \AA}$ , which is consistent with similar measurements in bulk water. This is striking because it suggests that the jump behavior of diffusing water is bulk-like despite the fact that it is within a nanoporous membrane. Similar observations have been made in other systems such as water confined in mesoporous silicon (mp-Si).<sup>23</sup> However, we also note that  $\langle l \rangle$  is larger in the AEM, on the order of  $5 \text{ \AA}$ , which is an observation we discuss later in the manuscript.

In addition to determining  $\langle l \rangle$  and  $\tau$ , QENS provides information about the fraction of non-diffusing species ( $f_{ND}$ ) as well as an estimate for the volume of the confinement in which a hydrogen atom moves within the time-scale of the QENS measurement. By assuming the water is freely diffusing within a volume represented as a sphere, the characteristic confinement radius ( $a$ ) can be estimated using the following relationship between  $EISF$  and  $a$ , which is determined by the ratio of the elastically scattered intensity to the sum of the

total elastic and quasi-elastic scattering intensities ( $x$  defined in Eq. 3),

$$\begin{aligned} x &= EISF \\ &= f_{ND} + (1 - f_{ND}) \left( \frac{3j_1(Qa)}{Qa} \right)^2, \end{aligned} \quad (6)$$

$$j_1(Qa) = \frac{\sin(Qa)}{Qa} - \frac{\cos(Qa)}{Qa}. \quad (7)$$

The  $EISF$  and corresponding fits for AEM and DM at room temperature measured by DCS are shown in Fig. 5. The fit parameters at multiple temperatures are summarized in Table 2. The water content within the two materials is significantly different, so it is difficult to draw any conclusions from the comparison of the absolute  $f_{ND}$  values.

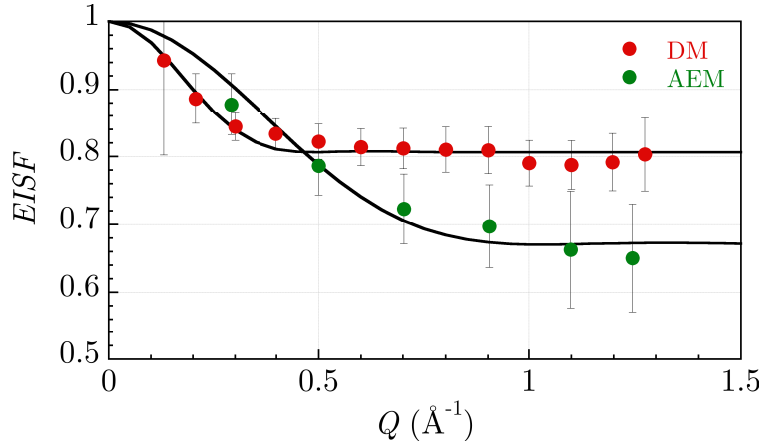


Figure 5: Elastic incoherent structure factor ( $EISF$ ) vs. ( $Q$ ) for AEM and DM at room temperature. Error bars represent one standard deviation.

We can comment on the temperature dependence of  $f_{ND}$  between the two materials as they display different behavior. Specifically,  $f_{ND}$  for AEM decreases significantly with increasing temperature whereas there is little change in  $f_{ND}$  for DM over a similar temperature window. This is consistent with a thermally activated process in the AEM where water is more strongly coupled to the polymer matrix, despite the overall larger water content. We also see that  $a$  is significantly smaller for AEM compared with DM ( $\approx 4 \text{ \AA}$  vs.  $\approx 9 \text{ \AA}$ ). This

Table 2: Extrapolated parameters from the QENS measurements for the AEM and DM.

	$T$ (K)	$\tau$ (ps)	$\langle l \rangle$ (Å)	$D$ ( $\times 10^{-9}$ m <sup>2</sup> /s)	$a$ (Å)	$f_{ND}$
AEM	303	39	4.4	0.82	4.4	0.67
	333	35	5.6	1.50	4.0	0.62
	348	26	5.6	2.05	4.2	0.38
DM	278	10.1	3.2	1.40	8.5	0.80
	298	9.8	3.5	2.06	9.3	0.81
	318	6.4	3.3	2.80	9.0	0.78

suggests that despite the significantly lower water content within DM, the water molecules within this membrane are less confined (larger confinement volumes  $\approx a^3$ ) compared with AEM. This is also consistent with a stronger coupling of the water dynamics to the polymer matrix in the case of the AEM. The temperature dependent  $f_{ND}$  for AEM would indicate that water dynamics are strongly coupled with that of the AEM polymer via strong ionic interactions. Yet this behavior is not observed for DM. The fact that  $f_{ND}$  is temperature independent strongly supports the notion that the motions of water are not coupled with motions of the DM within the time-scale of the QENS measurement thus the water dynamics within DM is inconsistent with the solution-diffusion model.

Using the fitting parameters from Table 2, the water diffusion coefficients for AEM and DM are calculated based on the jump diffusion model,<sup>24</sup>

$$D_{jump} = \frac{\langle l^2 \rangle}{6\tau}. \quad (8)$$

The corresponding values are compared with other materials from the literature including bulk water measured by QENS,<sup>25</sup> pulse field gradient nuclear magnetic resonance (NMR),<sup>26</sup> water confined in mp-Si membrane (pore size = 14 Å)<sup>23</sup> and a proton exchange membrane (Nafion<sup>®</sup>)<sup>27</sup> (Fig. 6). The water diffusion coefficients measured from NMR and QENS are in good agreement with each other and is consistent with that of bulk or free water diffusion. When water is confined in nanoporous channels, such as the case for the mp-Si, the water

diffusion coefficient becomes slightly depressed for temperatures above 280 K but is generally of the same order of magnitude.

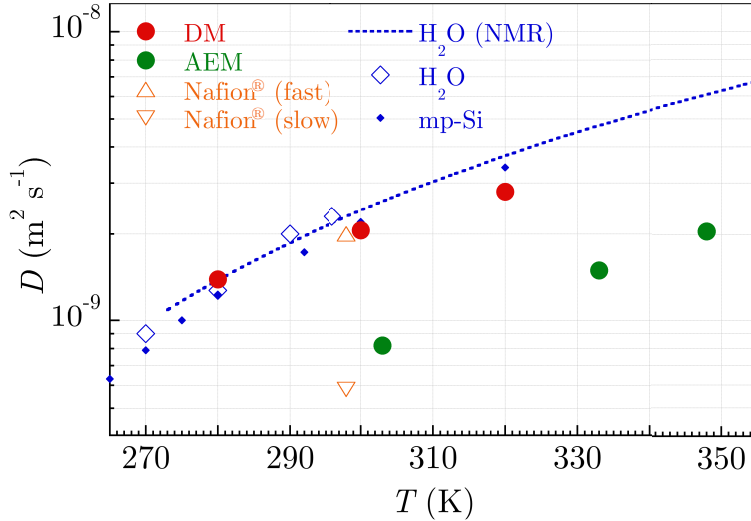


Figure 6: Comparison of the self-diffusion coefficients ( $D$ ) vs. temperature ( $T$ ) of water for AEM and DM measured in this study. Also included in this plot are self-diffusion coefficients for other materials reported in literature.

Nafion<sup>®</sup> is a unique material as two distinct water diffusion coefficients have been measured from QENS and are confirmed by NMR.<sup>27,28</sup> The slower water diffusion coefficient is a factor of 4 times lower than that of bulk water. It was suggested that this is related to confined or restricted diffusion of the water molecules forming a close hydration shell in proximity to the sulfonic acid functional groups of Nafion<sup>®</sup>. The faster water diffusion coefficient has a value very similar to that for bulk water. Here, it was suggested to be associated with fast water dynamics far away from the sulfonic acid groups, i.e. at or near the center of the ionic domain, where water channels are formed ( $\xi \approx 10 \text{ \AA}$ ) and the water molecules experiences bulk-like motions.

The water dynamics in AEM share some similarities to the local confined water motions found in Nafion<sup>®</sup>. At maximum swelling, SANS reveals that the block copolymer microdomains have a characteristic length-scale of  $\xi_1 \approx 63.8 \text{ \AA}$ . This length-scale is significantly larger than  $a$  observed in QENS, which would imply that the ionic aggregates inside the PVBTMA domains, and not the PVBTMA domains themselves, are constraining water

diffusion. It is likely that there is a distribution of water mobility inside the PVBTMA domains due to these ionic aggregates. We do not see two distinct water diffusion coefficients as seen in Nafion<sup>®</sup>. Instead only one water diffusion coefficient is observed for the AEM because the polymer content in the PVBTMA microdomain at maximum swelling is  $\approx 77\%$ , which is fairly high. However, we do not observe bulk water diffusion like in the case of Nafion<sup>®</sup> that swells to an even larger extent ( $\approx 35\%$  vs.  $\approx 10\%$ )<sup>29</sup> and forms bulk water channels at maximum swelling.

Unlike the AEM, the DM exhibits a water diffusion coefficient similar to that of free water over the measured temperature range. This is quite surprising as it is often argued that the water transport mechanism for water desalination membranes occur via a solution-diffusion process, which generally implies that the water motions are facilitated by segmental relaxations of the polymer. Our results show that the water motions are not coupled with the polymer dynamics, which is a key assumption for the solution-diffusion model. Thus the mechanism of transport is inconsistent with the solution-diffusion model since the DM is still well in the glassy state even when fully hydrated, and we observed that water diffuses as free water within the time- and length-scales probed by QENS. An alternative explanation is the water molecules are diffusing through the DM network heterogeneities,<sup>13</sup> which effectively functions as water channels whose dimensions are larger than the characteristic length-scale probed by QENS, which is  $\approx 10 \text{ \AA}$ . Specifically, the correlation lengths measured by SANS suggests that these water channels within the hydrated DM membrane  $\xi_2 \approx 27.2 \text{ \AA}$ , and is comparable with the characteristic radius measured by QENS,  $\xi_2 \approx 2a$ . The presence of water channels was recently demonstrated by molecular dynamics simulation of a similar DM membrane.<sup>30</sup>

The next logical question is why do bulk measurements of water diffusion through the same DM materials, via water permeation tests, exhibit a significantly lower water diffusion coefficient<sup>8</sup>? It is clear that the presence of the DM adds impedance to the transport process and slows down the diffusion through the membrane. We believe that this is a reflection

of the relevant length-scales of the measurements. It is critical to recognize that QENS measures diffusion over length-scales on the order of a nanometer or less. This length-scale is commensurate with intermolecular interactions, and therefore appropriate for studying the molecular mechanisms of transport. At these molecular length-scales, the structure of the DM does not add molecular impedance to the transport process; the AEM does. Over larger length-scales, the morphology and connectivity of the network heterogeneities that are present in the DM increase the impedance to the transport process. This is consistent with a hydrodynamic model of transport for DM and a molecular scale solution-diffusion model in the AEM.

## Conclusion

We can make several major points from our results. As expected, the operative mechanism of transport for the AEM membrane [studied here](#) appears to be the solution-diffusion model where the presence of the ionic groups solubilizes the water upon hydration. Despite the fact that DM swells upon hydration, the operative transport mechanism appears to be pore flow. Water moves freely in the network heterogeneities of the DM, in a manner that is analogous in a rigid mesoporous silicate membrane that does not swell at all. This seminal insight suggests the notion of the DM as the perm-selective active layer is inaccurate as the pore flow mechanism seems more consistent with our results. One caveat to this conclusion is that this study is focused on a specific water desalination membrane and future work will address this by applying similar measurements to study the transport mechanism of water desalination membranes containing other functional moieties.

Finally, our results have implications in the design of future water desalination membranes. Currently, there is a drive towards designing nanoporous membranes for enhanced water permeation by leveraging convective transport. Many materials platforms, such as carbon nanotubes, aquaporin derivatives or nanoporous block copolymers, are being proposed

yet the implementation of most of these materials are challenged by scalability. The results presented here suggest that the DM membranes already leverage this mechanism of transport albeit not as idealized because of the convective pathways are most likely more tortuous compared to the proposed replacement materials. Nevertheless, we should not overlook DM membranes as they are already scalable. Perhaps the focus should be towards improving current materials by reducing the tortuosity of their convective pathways, via better control over the polymer network structure, to improve permeance.

## Acknowledgement

The authors thank the NIST Center for Neutron Research (NCNR) and Neutrons for Soft Matter (nSOFT) for access to the neutron scattering facilities. Access to the HFBS instrument was provided by the Center for High Resolution Neutron Scattering (CHRNS), a partnership between the NIST and the National Science Foundation under Agreement No. DMR-1508249. J.D.T. gratefully acknowledges support from the US DOE Office of Energy Efficiency and Renewable Energy, Fuel Cell Technologies Office, under Contract No. DE-AC36-08GO28308. The authors thank Dow Chemical for providing the DM materials. The AEM was prepared under sponsorship by the US Army under MURI grant number W911NF-10-1-0520. E.P.C. thanks Dr. Katie Feldman, Dr. Antonio Faraone and Dr. Wen-Li Wu for providing invaluable comments to the manuscript. This work is a contribution of NIST, an agency of the U.S. Government, and not subject to U.S. copyright.

## Supporting Information Available

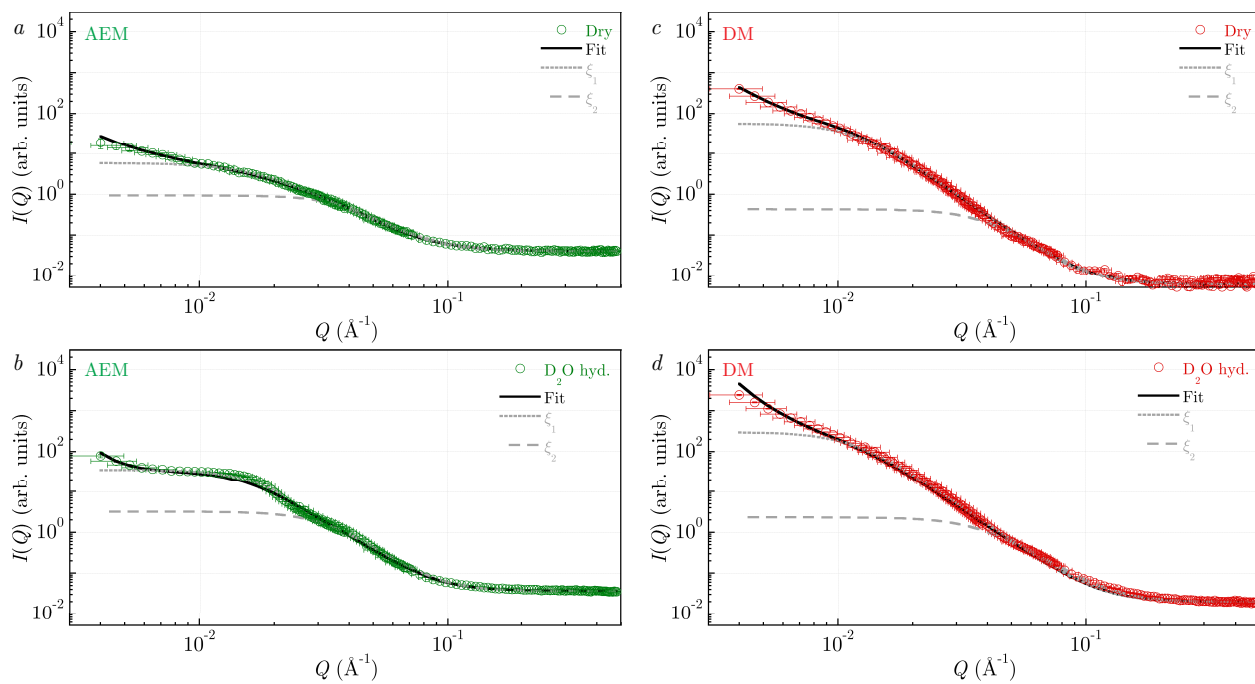


Figure S1:  $I(Q)$  vs.  $Q$ , along with fits of the correlation lengths, for a) dry AEM, b) AEM hydrated with  $D_2O$ , c) dry DM, and d) DM hydrated with  $D_2O$ . Error bars represent one standard deviation.

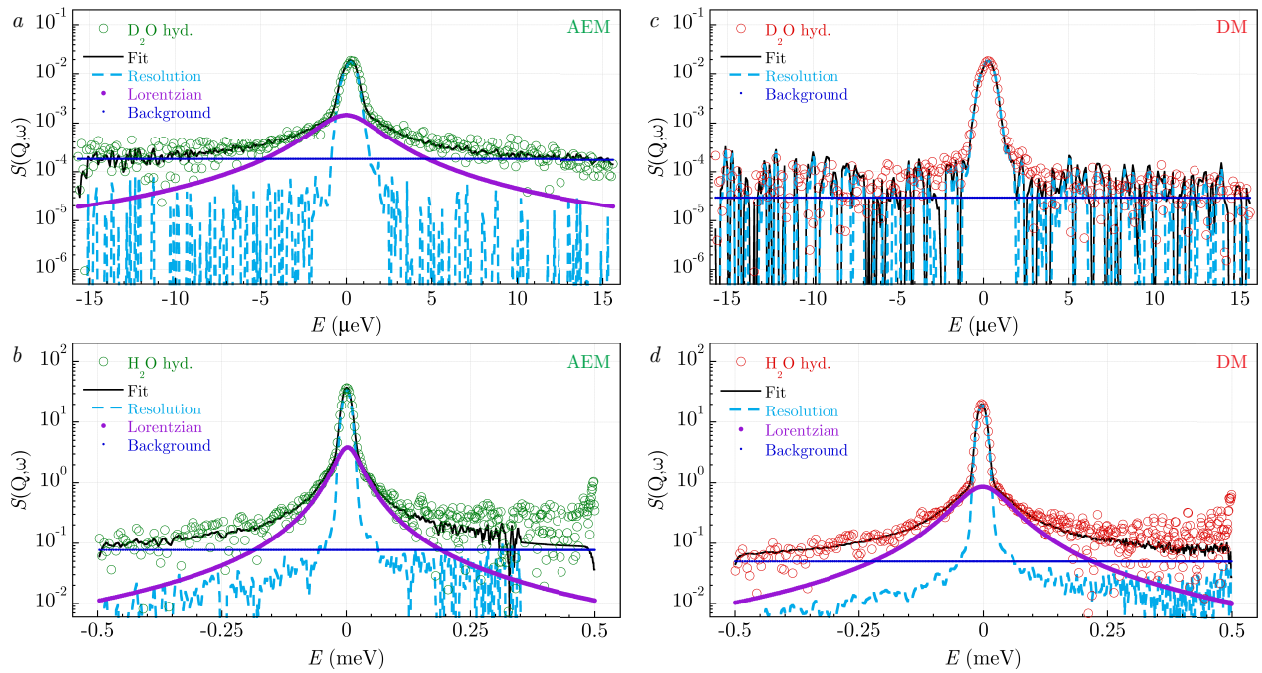


Figure S2: a)  $S(Q, \omega)$  vs.  $E$  from HFBS for AEM that is hydrated with  $\text{H}_2\text{O}$ .  $S(Q, \omega)$  vs.  $E$  from DCS for AEM that is hydrated with  $\text{D}_2\text{O}$ . c)  $S(Q, \omega)$  vs.  $E$  from HFBS for DM that is hydrated with  $\text{H}_2\text{O}$ . d)  $S(Q, \omega)$  vs.  $E$  from DCS for DM that is hydrated with  $\text{D}_2\text{O}$ .

## References

- (1) Freeman, B. D. Basis of Permeability/Selectivity Tradeoff Relations in Polymeric Gas Separation Membranes. *Macromolecules* **1999**, *32*, 375–380.
- (2) Lonsdale, H. K.; Merten, U.; Riley, R. L. Transport properties of cellulose acetate osmotic membranes. *J. Appl. Polym. Sci.* **1965**, *9*, 1341–1362.
- (3) Geise, G. M.; Lee, H.; Miller, D. J.; Freeman, B. D.; McGrath, J. E.; Paul, D. R. Water purification by membranes: The role of polymer science. *J. Polym. Sci. B* **2010**, *48*, 1685–1718.
- (4) Meares, P. On the mechanism of desalination by reversed osmotic flow through cellulose acetate membranes. *Eur. Polym. J.* **1966**, *2*, 241–254.
- (5) Lin, L.; Lopez, R.; Ramon, G. Z.; Coronell, O. Investigating the void structure of the polyamide active layers of thin-film composite membranes. *J. Membr. Sci.* **2016**, *497*, 365–376.
- (6) Baker, R. *Membrane Technology and Applications*; John Wiley & Sons, 2004.
- (7) Yasuda, H.; Peterlin, A. Diffusive and bulk flow transport in polymers. *J. Appl. Polym. Sci.* **1973**, *17*, 433–442.
- (8) Geise, G. M.; Park, H. B.; Sagle, A. C.; Freeman, B. D.; McGrath, J. E. Water permeability and water/salt selectivity tradeoff in polymers for desalination. *J. Membr. Sci.* **2011**, *369*, 130–138.
- (9) Chan, E. P.; Young, A. P.; Lee, J.-H.; Stafford, C. M. Swelling of Ultrathin mLbL Polyamide Water Desalination Membranes. *J. Polym. Sci. B Polym. Phys.* **2013**, *51*, 1647–1655.
- (10) Zhang, W. Synthesis and Characterization of Polymeric Anion Exchange Membranes. Ph.D. thesis, University of Massachusetts Amherst, 2016.

- (11) Kline, S. R. Reduction and analysis of SANS and USANS data using IGOR Pro. *Journal of Applied Crystallography* **2006**, *39*, 895–900.
- (12) Azuah, R. T.; Kneller, L. R.; Qiu, Y.; Tregenna-Piggott, P. L. W.; Brown, C. M.; Copley, J. R. D.; Dimeo, R. M. DAVE: A Comprehensive Software Suite for the Reduction, Visualization, and Analysis of Low Energy Neutron Spectroscopic Data. *J Res Natl Inst Stand Technol* **2009**, *114*, 341–358.
- (13) Chan, E. P.; Young, A. P.; Lee, J.-H.; Chung, J. Y.; Stafford, C. M. Swelling of Ultrathin Crosslinked Polyamide Water Desalination Membranes. *J. Polym. Sci. B Polym. Phys.* **2013**, *51*, 385–391.
- (14) Chan, E. P.; Lee, S. C. Thickness-Dependent Swelling of Molecular Layer-by-Layer Polyamide Nanomembranes. *J. Polym. Sci. B Polym. Phys.* **2017**, *55*, 412–417.
- (15) Sunday, D. F.; Chan, E. P.; Orski, S. V.; Nieuwendaal, R. C.; Stafford, C. M. Functional group quantification of polymer nanomembranes with soft x-rays. *Phys. Rev. Materials* **2018**, *2*, 032601.
- (16) Hammouda, B.; Ho, D.; Kline, S. SANS from Poly(ethylene oxide)/Water Systems. *Macromolecules* **2002**, *35*, 8578–8585.
- (17) Shibayama, M. Small-angle neutron scattering on polymer gels: phase behavior, inhomogeneities and deformation mechanisms. *Polym J* **2011**, *43*, 18–34.
- (18) Matsunaga, T.; Sakai, T.; Akagi, Y.; Chung, U.-i.; Shibayama, M. SANS and SLS Studies on Tetra-Arm PEG Gels in As-Prepared and Swollen States. *Macromolecules* **2009**, *42*, 6245–6252.
- (19) Saffer, E. M.; Lackey, M. A.; Griffin, D. M.; Kishore, S.; Tew, G. N.; Bhatia, S. R. SANS study of highly resilient poly(ethylene glycol) hydrogels. *Soft Matter* **2014**, *10*, 1905–1916.

- (20) Meyer, A.; Dimeo, R. M.; Gehring, P. M.; Neumann, D. A. The high-flux backscattering spectrometer at the NIST Center for Neutron Research. *Rev. Sci. Instrum.* **2003**, *74*, 2759–2777.
- (21) Copley, J. R. D.; Cook, J. C. The Disk Chopper Spectrometer at NIST: a new instrument for quasielastic neutron scattering studies. *Chemical Physics* **2003**, *292*, 477–485.
- (22) Hall, P. L.; Ross, D. K. Incoherent neutron scattering functions for random jump diffusion in bounded and infinite media. *Mol. Phys.* **1981**, *42*, 673–682.
- (23) Chen, S.-H.; Mallamace, F.; Mou, C.-Y.; Broccio, M.; Corsaro, C.; Faraone, A.; Liu, L. The violation of the Stokes–Einstein relation in supercooled water. *PNAS* **2006**, *103*, 12974–12978.
- (24) Singwi, K. S.; Sjölander, A. Diffusive Motions in Water and Cold Neutron Scattering. *Phys. Rev.* **1960**, *119*, 863–871.
- (25) Mitra, S.; Mukhopadhyay, R.; Tsukushi, I.; Ikeda, S. Dynamics of water in confined space (porous alumina): QENS study. *J. Phys.: Condens. Matter* **2001**, *13*, 8455.
- (26) Holz, M.; Heil, S. R.; Sacco, A. Temperature-dependent self-diffusion coefficients of water and six selected molecular liquids for calibration in accurate  $^1\text{H}$  NMR PFG measurements. *Phys. Chem. Chem. Phys.* **2000**, *2*, 4740–4742.
- (27) Perrin, J.-C.; Lyonnard, S.; Volino, F. Quasielastic Neutron Scattering Study of Water Dynamics in Hydrated Nafion Membranes. *J. Phys. Chem. C* **2007**, *111*, 3393–3404.
- (28) Pivovar, A. M.; Pivovar, B. S. Dynamic Behavior of Water within a Polymer Electrolyte Fuel Cell Membrane at Low Hydration Levels. *J. Phys. Chem. B* **2005**, *109*, 785–793.
- (29) Nadermann, N. K.; Davis, E. M.; Page, K. A.; Stafford, C. M.; Chan, E. P. Using Indentation to Quantify Transport Properties of Nanophase-Segregated Polymer Thin Films. *Adv. Mater.* **2015**, *27*, 4924–4930.

- (30) Kawakami, T.; Nakada, M.; Shimura, H.; Okada, K.; Kimura, M. Hydration structure of reverse osmosis membranes studied via neutron scattering and atomistic molecular simulation. *Polym. J.* **2018**, 1.

# Graphical TOC Entry

Small-angle and quasi-elastic neutron scattering methods are used to study the structure as well as the water and polymer dynamics of several polymeric membranes to show that water diffuses through a water desalination membrane (DM) comparable to bulk water whereas water diffuses by a factor of two slower in an anion exchange membrane (AEM). These findings are reconciled in the context of the unique transport mechanism for the two materials. Specifically, the DM possesses a tortuous network of nanopores whereas the AEM is a swollen network without such channels. This level of insight is critical for designing new and improved transport membranes.

